Low-temperature positron annihilation study of B+-ion implanted PMMA

ARTICLE *in* LOW TEMPERATURE PHYSICS · AUGUST 2014

Impact Factor: 0.79 · DOI: 10.1063/1.4892646

8 AUTHORS, INCLUDING:

O. Šauša

Slovak Academy of Sciences

52 PUBLICATIONS **373** CITATIONS

SEE PROFILE

Yury Nicolaevich Osin

Kazan (Volga Region) Federal University

74 PUBLICATIONS **331** CITATIONS

SEE PROFILE

Andrey L. Stepanov

Russian Academy of Sciences

244 PUBLICATIONS **2,655** CITATIONS

SEE PROFILE

THE JOURNAL OF PHYSICAL CHEMISTRY B

Article

pubs.acs.org/JPCB

Structural Defects and Positronium Formation in 40 keV B^+-Implanted Polymethylmethacrylate

Taras Kavetskyy,*[,†] Volodymyr Tsmots,[†] Atsushi Kinomura,[‡] Yoshinori Kobayashi,[‡] Ryoichi Suzuki,[‡] Hamdy F. M. Mohamed,[§] Ondrej Šauša,[∥] Vladimir Nuzhdin,[⊥] Valery Valeev,[⊥] and Andrey L. Stepanov[⊥]

[†]Faculty of Biology and Solid-State Microelectronics Laboratory, Drohobych Ivan Franko State Pedagogical University, 24 I. Franko Str., Drohobych 82100, Ukraine

[‡]Research Institute of Instrumentation Frontier, National Institute of Advanced Industrial Science and Technology (AIST), Tsukuba, Ibaraki 305-8568, Japan

[§]Physics Department, Faculty of Science, Minia University, P.O. Box 61519, Minia, Egypt

[∥]Institute of Physics of Slovak Academy of Sciences, Dúbravská cesta 9, Bratislava 84511, Slovak Republic

[⊥]Kazan Physical-Technical Institute of Russian Academy of Sciences, 10/7 Sibirskiy trakt, Kazan 420029, Russian Federation

ABSTRACT: Slow positron beam and optical absorption measurements are carried out to study structural defects and positronium formation in 40 keV B^+-implanted polymethylmethacrylate (B:PMMA) with ion doses from 6.25×10^{14} to 5.0×10^{16} ions/cm^2. Detailed depth-selective information on defects in implanted samples was obtained by measuring of Doppler broadening of positron annihilation γ rays as a function of incident positron energy and these experimental results were compared with SRIM (stopping and range of ions in matter) simulation results. Two general processes, appearance of free radicals at lower ion doses (<10^{16} ions/cm^2) and carbonization at higher ion doses (>10^{16} ions/cm^2), are considered from the Doppler $S-E$ and $W-E$ dependences in the framework of the concept of defects formation during radiation damage of polymer structure. Probabilities of *ortho*-positronium (*o*-Ps) formation are analyzed using $S-W$ plot and slow positron annihilation lifetime measurements. Dose dependence of *o*-Ps lifetime τ_3 and intensity I_3 at the incident positron energy of 2.15 keV correlates well with the dose dependence of *S*-parameter and seems to account for the existence of the expected two processes, i.e., scission of polymer chains and appearance of free radicals preceding the aggregation of the clusters resulting in the formation of network of conjugated bonds at lower ion doses and carbonization at higher ion doses. The increase of optical absorption observed with increasing ion implantation dose also suggests a formation of carbonaceous phase in the ion-irradiated PMMA.

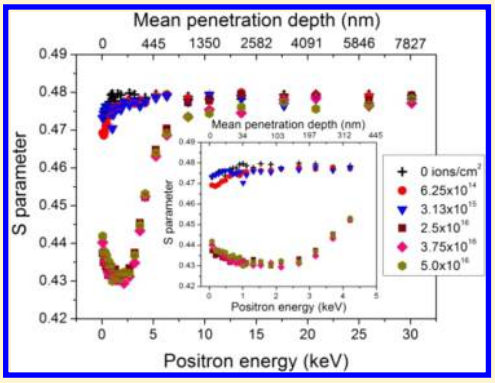

1. INTRODUCTION

Ion implantation of polymers is a subject of stimulating and growing investigations from past to modern time.[1−11] The interest to ion-irradiated polymers is due to the ion implantation being one of the effective technological methods to turn dielectric polymers into conducting semiconductors.[2,3] In this context, Sviridov[8] reviewed the main chemical aspects of structural modification by ion implantation of polymeric materials. Namely, long-term ion bombardment of a polymer by various ions causes essential transformations of the material, accompanied by the formation of amorphous hydrogenated carbon inside polymers, which exhibits strong conducting properties. Thus ion irradiation is responsible for an increase in the conductivity of initially dielectric polymers (for example, polyimide and polyethylene) by 10−18 orders of magnitude.[8] Investigations carried out in the past decade demonstrated that varying the main parameters of ion irradiation (such as energy and mass of implanted ions, implantation dose, ion current density, etc.) gives a significant impact on the formation of carbonaceous conductive phase in the implanted polymer layers.

It has been reviewed[9,10] that the implantation-induced structural changes of polymers result in the scission and cross-linking of polymer chains, formation of volatile low-molecular-weight fragments followed by their degassing and carbonization of the implanted layer. In particular, the carbonization process occurs at several stages with an increase of implantation dose or/and ion current density: (i) formation of "pre-carbon" structures; (ii) nucleation and growth of the carbon-enriched clusters; (iii) aggregation of the clusters resulting in the formation of network of conjugated bonds; (iv) transition to amorphous carbon or graphite-like material. It was recognized that the carbonization process depends mainly on the ion dose, current density, and energy and to a smaller extent ion species (only in the sense of

Received: October 31, 2013
Revised: January 14, 2014
Published: January 27, 2014

ion mass). However, it is not completely clear at present how the carbonaceous phase formed under the high-dose implantation could be dependent on the type of polymer.

Some efforts have been made by researchers to study the B^+ implantation in various polymers such as polyethylene (PE), polyamide (PA), polyimide (PI), cellulose (CL), and poly-(ethylene terephthalate) (PET).[4−7] As a result, the concept of appearance of a carbonized ion-implanted layer, which takes into account the formation of low unsaturated compounds, primitive carbon clusters, followed by carbon cluster nucleation and growth of conducting carbon "drops" with saturated and unsaturated (conjugate) intercluster bridge bonds being capable of efficient charge exchange (carbon conductive layer), has been developed; this is a significant fundamental and practical contribution in the field of conductive polymer science. In some publications it has been also assumed that such a carbon conductive layer can be the basis of the qualitatively new electrical properties of implanted polymer materials. Unfortunately, B^+ implantation of widely used in practice polymer polymethylmethacrylate (PMMA) (B:PMMA) was not studied so far.

On the other hand, PMMA is very useful material for construction of many optical components such as waveguides, lenses, prisms, etc. Particularly, this polymer was also a subject for implantation with Ag^+ ions to fabricate composite structures with silver nanoparticles for plasmonic applications.[11] Additionally, in the case of B:PMMA it could be suggested that study of such composition is important not only from the position of the fundamental science of irradiation of the polymer but also in a practical viewpoint similar to C^+, N^+, and Ar^+ implantation into PMMA.[12,13] In particular, it has been shown that C^+ implantation into PMMA may be potentially of interest for fabrication of organic luminescent devices, backlight components in liquid crystal display systems, and diffractive elements and micro-components for integrated optical circuits.[12] N^+ and Ar^+ implantation into PMMA demonstrates a drastic change in its optical parameters (the values of optical energy gap decrease while those for refractive index increase with the increasing dose of implanted ions) that may find an extensive application in fabrication of various opto-electronic devices including organic light emitting diodes, solar cells, waveguides, etc.[13]

In principle, two processes could be expected by B^+ implantation into PMMA: (i) formation of structural defects by radiation damage of polymer chains and appearance of free radicals at rather lower ion doses (for instance $<10^{16}$ ions/cm^2), and (ii) carbonization effects at higher ion doses (for instance $>10^{16}$ ions/cm^2). Approximately at a dose of 10^{16} ions/cm^2, a carbon phase in various implanted polymers begins to be formed.[10] To examine such concept of structural modification of B:PMMA, slow positron beam spectroscopy (SPBS)[14,15] could be a useful tool for obtaining depth-selective information on volume defects upon ion implantation.

The experimental SPBS technique and sometimes together with the SRIM (stopping and range of ions in matter) simulation of ion profile distribution have already been successfully applied for analyzing inorganic materials implanted by various ions such as H:Si,[16] Er:SiO_2/Si,[17,18] He:Si,[19] Al:ZnO,[20] H:ZnO,[21] N:ZnO,[22,23] He−H:Si,[24,25] Ge:Ge and Si:Ge,[26,27] H:GaN,[28] N:Si,[29] Li:ZnO,[30] Na:ZnO,[31] etc.

In our case of B:PMMA, additionally to depth-resolved defect distribution, the information on the positronium (Ps) formation (the metastable electron-positron bound state)[32,33] can be also extracted. It should be noted that the SPBS technique will be applied to study ion-implanted PMMA for practical use for the first time. As mentioned above, B:PMMA will be considered to demonstrate an efficiency of this experimental approach. In addition, some information on the ion irradiation defects in B:PMMA could be supported by optical absorption observations.

Thus, the present work is aimed to study the depth-resolved defects and Ps formation in 40 keV B^+-implanted PMMA with ion doses from 6.25×10^{14} to 5.0×10^{16} ions/cm^2 using SPBS, optical absorption measurements and SRIM simulation. The article is organized as follows. Experimental and simulation details are described in section 2. In section 3, the results and discussion are presented on SPBS and SRIM simulation in subsection 3.1 and optical absorption in subsection 3.2. Finally, conclusions are drawn in section 4.

2. EXPERIMENTAL SECTION

As substrates for low energy ion implantation, 1.2-mm-thick PMMA plates were used, which are optically transparent in a wide spectral range 400−1000 nm.[9] B^+ implantation (the energy 40 keV, doses from 6.25×10^{14} to 5.0×10^{16} ions/cm^2, and ion current density <2 μA/cm^2) was performed under a pressure of 10^{-5} Torr at room temperature on an ILU-3 ion accelerator at the Kazan Physical-Technical Institute (KPTI, Russia).[9]

SPBS measurements were carried out at the National Institute of Advanced Industrial Science and Technology (AIST, Japan).[34] Doppler broadening spectra (i.e., S−E or W−E curves) were measured by a slow-positron beamline with a radioactive ^{22}Na positron source and a semiconductor detector. The positron incident energy E was changed in the range from 0 to 30 keV. The S parameter was determined as the ratio of the counts in the window ±0.7 keV from the center of the annihilation peak to the total counts contained in the peak (±4.2 keV from the center of the annihilation peak). The W parameter was determined as the ratio of the counts in the window ±(1.8−4.2) keV from the center of the peak to the total counts contained in the peak. Positron annihilation lifetime spectra were measured by another beamline using an electron linear accelerator as an intense slow-positron source. For lifetime measurements, positron pulses were formed by a combination of chopper and buncher electrodes.[35] Annihilation γ-rays were detected by a BF_2 scintillator and a photomultiplier tube. The positron energy for lifetime measurements was determined on the basis of the Doppler broadening spectra. The total number of accumulated counts was 10^6. A time resolution of 0.25 ns at fwhm was obtained.

TRIM (transport of ions in matter) code simulations were conducted using the software of version SRIM-2012[36] to obtain the depth profile of implanted ions and radiation-induced vacancies during 40 keV B^+ implantation into PMMA. These modeling results will be compared with experimental SPBS data. To date, only one paper concerns SRIM and SPBS comparative analysis for ion-irradiated polymer,[37] where 2 MeV Au^+- and O^+-irradiated poly(aryl ether ether ketone) (PEEK) samples have been studied. In this respect, the additional SRIM simulations for 40 keV Au^+ and O^+ implantation of PMMA are performed and shown here to be compared with the conclusions of the work of Hirata et al.[37]

Optical absorption measurements were conducted in the wavelength range 200−800 nm using a SHIMADZU UV-3100PC spectrophotometer (AIST, Japan).

dx.doi.org/10.1021/jp410763t | J. Phys. Chem. B 2014, 118, 4194−4200

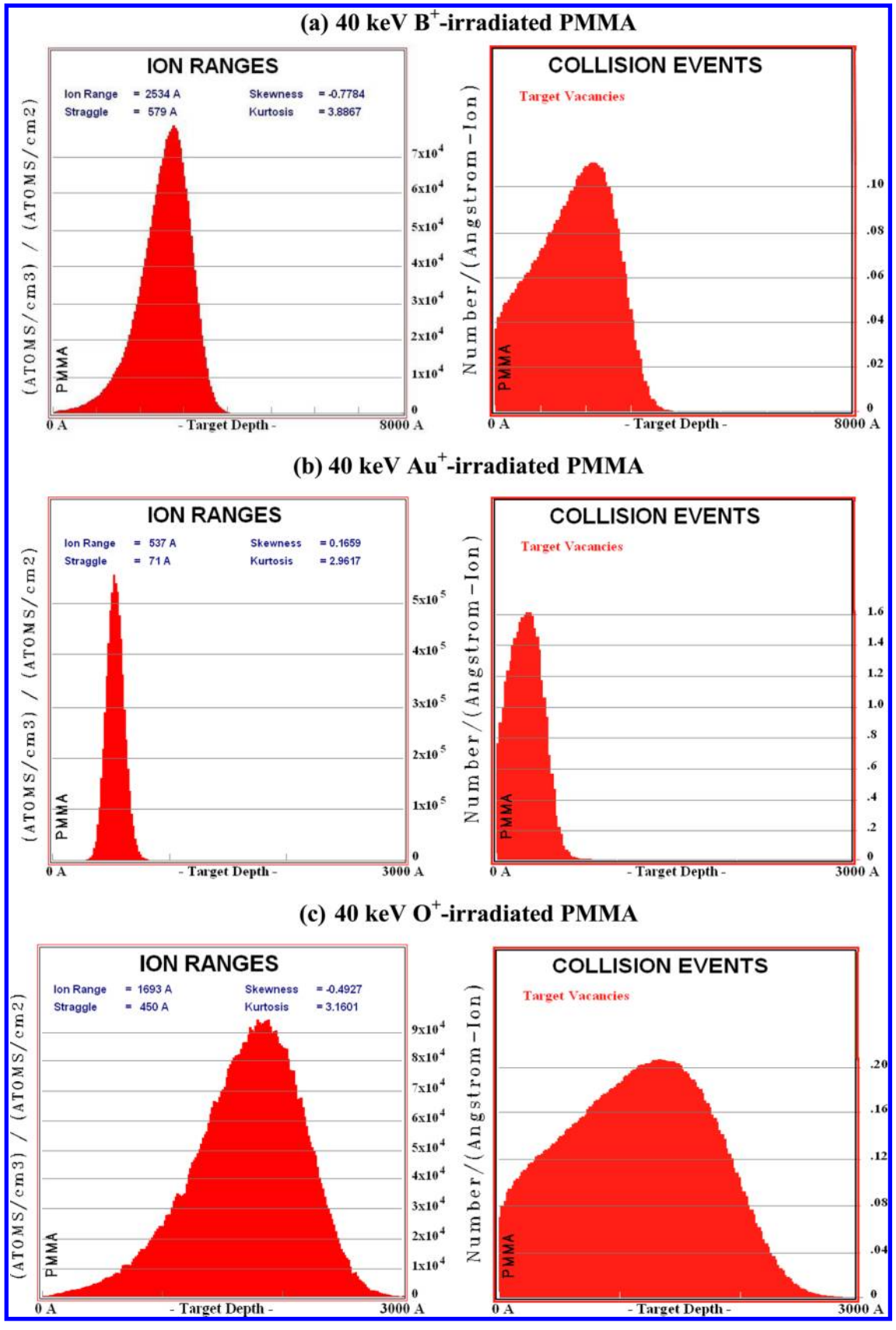

Figure 1. SRIM simulations of the depth profiles of implanted ions (left) and introduced vacancies (right) for the 40 keV B^+-irradiated PMMA (a, top), Au^+-irradiated PMMA (b, middle), and O^+-irradiated PMMA (c, bottom).

dx.doi.org/10.1021/jp410763t | J. Phys. Chem. B 2014, 118, 4194−4200

3. RESULTS AND DISCUSSION

3.1. Slow Positron Beam Spectroscopy and SRIM Simulation. Figure 1 presents the depth distributions of implanted ions and vacancies in PMMA calculated by SRIM. The numerical values of simulation results are gathered in Table 1. As seen from a simulation of B:PMMA (Figure 1, top),

Table 1. SRIM Simulation Results for B^+, Au^+, and O^+ Implantation into PMMA

sample	energy	R_{max}^{ion}, nm	R_p^{ion}, nm	R_{max}^{V}, nm	R_p^{V}, nm
B:PMMA	40 keV	400	253	380	220
Au:PMMA	40 keV	75	54	60	25
O:PMMA	40 keV	300	170	280	150
Au:PEEK[a]	2 MeV		620		
O:PEEK[a]	2 MeV		2420		

[a]Modeling data from the work of Hirata et al.[37]

a mean penetration (R_p^B) range of 40 keV accelerated B^+-ions into the PMMA matrix is about R_p^B = 253 nm with a straggling (ΔR_p^B) of 58 nm and the maximum penetration (R_{max}^B) value is about R_{max}^B = 400 nm. It should be noted here that R_p is the most useful parameter in ion implantation research, and R_{max} is a value that characterizes the deepest level in an irradiated matrix for penetration of implanted ions and corresponds to a boundary in matrix between ion modified and virgin areas of PMMA. The SRIM modeling yielded a defect (vacancy) profile with a depth at the highest concentration of vacancies ($R_p^{V,B}$) (i.e., maximum damage) around $R_p^{V,B}$ = 220 nm, which extends into full depth of vacancies ($R_{max}^{V,B}$) (i.e., thickness of damaged layer) up to $R_{max}^{V,B}$ = 380 nm.

For simulation of Au:PMMA for 40 keV (Figure 1, middle) the ion profile extends up to about R_{max}^{Au} = 75 nm with the R_p^{Au} = 54 nm, whereas a vacancy distribution shows a maximum damage around $R_p^{V,Au}$ = 25 nm and depth up to around $R_{max}^{V,Au}$ = 60 nm. The close values to modeling data of B:PMMA are observed for modeling of O:PMMA for 40 keV (Figure 1, bottom), where the simulation demonstrates R_{max}^{O} = 300 nm with R_p^{O} = 170 nm, and vacancy profile with a maximum damage around $R_p^{V,O}$ = 150 nm and maximal depth up to around $R_{max}^{V,O}$ = 280 nm.

In the work of Hirata et al.[37] a radiation damage of Au:PEEK and O:PEEK for 2 MeV was experimentally analyzed by the variable-energy positron beams (i.e., SPBS). In the case of O:PEEK, the average implantation depth R_p = 2420 nm is found to be in good agreement with the thickness of damaged polymer layer between 2200 and 2800 nm in dependence of the ion dose, as seen from SPBS. On the other hand, for Au:PEEK a value of R_p = 620 nm is remarkably different from the experimental data 1200−1300 nm. In our case, the SRIM simulation results for B:PMMA and O:PMMA for 40 keV are very close (Figure 1, top and bottom; Table 1). Therefore, it could be suggested that ion implantation depth for B:PMMA will be also in consistence with the thickness of damaged polymer layer estimated by SPBS.

Figure 2 displays the dose dependence of S−E and W−E curves for unimplanted PMMA and B:PMMA. The mean penetration depth of positrons (z_m) is estimated using the formula[38]

$$z_m = (40/\rho)E^n \quad (1)$$

where z_m is presented in nm, E the positron energy in kiloelectronvolts, ρ is the density (1.18 g/cm^3 for PMMA), and n = 1.6. The positron energy range up to 5 keV corresponds to a depth 445 nm for the unimplanted PMMA. In the same region of

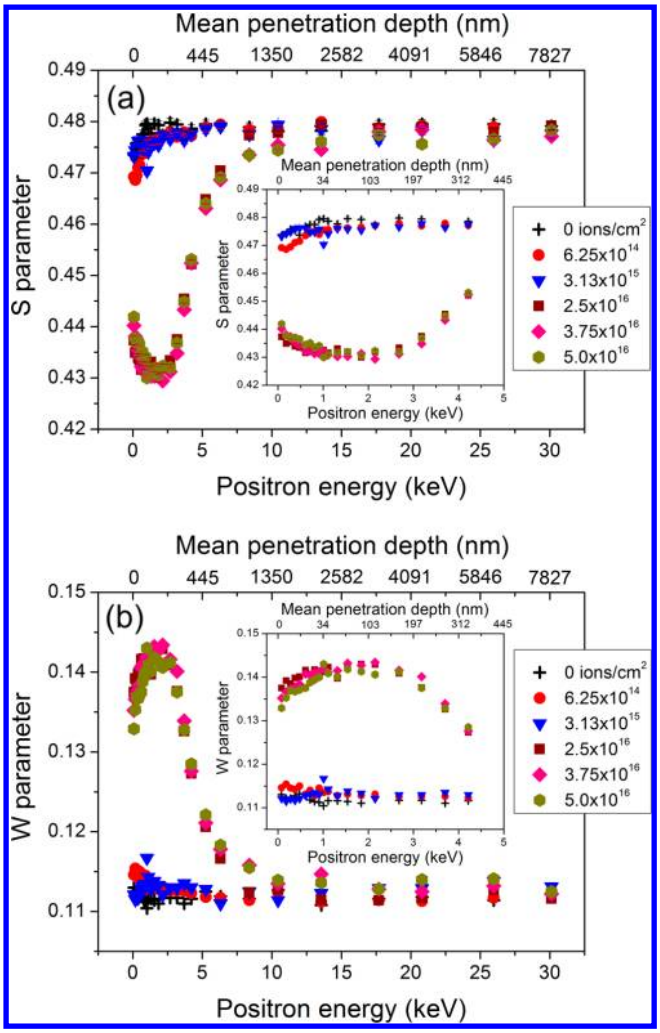

Figure 2. Dose dependence of S−E (a, top) and W−E (b, bottom) curves for B:PMMA. The error bars are within the size of the symbol.

depth the SRIM simulation predicts R_{max}^B = 400 nm in B:PMMA (Table 1). As one can see, the positron energy of 2−3 keV, at which S minimum and W maximum are observed, corresponds to z_m near 100−200 nm, which is rather close to the damaged layer ($R_p^{V,B}$ = 220 nm) of B:PMMA, as predicted also by SRIM (Figure 1, top and Table 1). Thus the observed changes of S and W parameters in the range 0.08−5 keV are connected with B^+-implanted layer. Saturation of S and W parameters in the positron energy range 6−30 keV is due to the positron annihilation in PMMA volume below the ion-implanted layer.

It is suggested, as typical for irradiated polymers,[4,5] at lower ion doses (6.25×10^{14} to 3.13×10^{15} ions/cm^2) after penetration of accelerated B^+ ions into PMMA, some polymer chains can be broken, resulting in the appearance of free radicals simultaneously with formation of free volume spaces in their vicinity between molecules after extraction of some oxygen and hydrogen atoms. At higher ion doses (2.5×10^{16} to 5.0×10^{16} ions/cm^2), the carbonization should take place in a case of PMMA likely as it has been demonstrated in literature for PMMA implanted by various gas ions.[13,39] Figure 3 shows dose dependence of S parameter at incident positron energies of 2.15 and 3.18 keV for the investigated B:PMMA. It is clearly seen that in both cases the S parameter decreases sharply when the ion dose exceeds 10^{16} ions/cm^2.

dx.doi.org/10.1021/jp410763t | J. Phys. Chem. B 2014, 118, 4194−4200

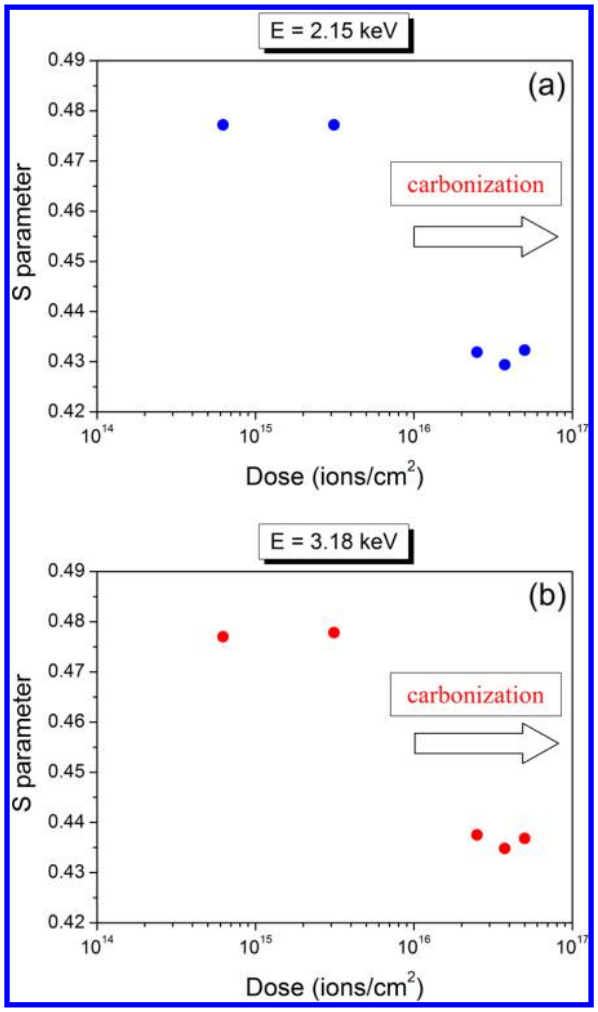

Figure 3. Dose dependence of *S* parameter at incident positron energies of 2.15 keV (a, top) and 3.18 keV (b, bottom) for B:PMMA. The error bars are within the size of the symbol; the arrows show carbonization at higher ion doses (see text for details).

Figure 4 demonstrates the dose dependence of *S*−*W* plots for B^+-implanted PMMA. Here, the *S*−*W* plot for Kapton foil is shown for comparison. Both the black and red lines show variations of *S* and *W* as a function of positronium yield.

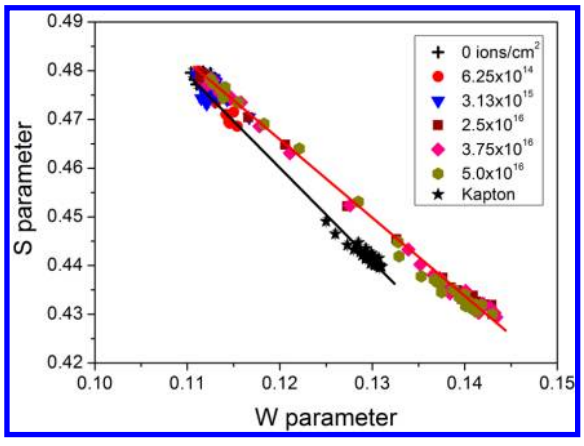

Figure 4. Dose dependence of *S*−*W* plots for B:PMMA. The *S*−*W* plot for Kapton foil is shown for comparison. The error bars are within the size of the symbol; the solid lines are drawn as a guide for the eye (see text for details).

In unimplanted PMMA, a good fraction of positrons form positronium, which raises *S* and reduces *W*. In oxygenated Kapton foil[40] no positronium forms so for this polymer *S* is low and *W* is high. The black line shows the correlation as function of positronium yield for polymers containing oxygen in its chemical structure (for polymers, for example, containing fluorine like polytetrafluoroethylene, it has been observed[40] that the correlation between *S* and *o*-Ps fraction has a slope much different from that for the oxygenated polymers). As for the red line, at high positron energy PMMA is intact and shows high *S* and low *W* due to a fairly large fraction of positronium. At low positron energies the polymer is heavily damaged so that positronium formation is much reduced. This is the reason for the lower *S* and higher *W* for high ion dose (>10^{16} ions/cm^2) at low incident energies for heavily damaged PMMA. As also seen from Figure 4, the slope of the red line is different from the black line. To explain this finding, we suggest that the electronic structure (or the composition) of the heavily damaged PMMA is different from that of Kapton foil. Perhaps oxygen in PMMA is removed from the damaged region and momentum distribution probed by the positrons is different from that in oxygenated Kapton foil.

To receive more information on the probabilities of *ortho*-positronium (*o*-Ps) formation in the near surface region of material, slow positron annihilation lifetime measurements at low incident positron energy were performed. The obtained *o*-Ps lifetime τ_3 and intensity I_3 data at the incident positron energy of 2.15 keV for the investigated B:PMMA are presented in Table 2.

Table 2. Positron Annihilation Lifetimes and Intensities at Incident Positron Energy of 2.15 keV

dose, B^+/cm^2	*o*-Ps lifetime, τ_3 (ns)	*o*-Ps intensity, I_3 (%)
0	1.765	35.0
6.25×10^{14}	1.752	34.6
3.13×10^{15}	1.752	34.8
2.5×10^{16}		no *o*-Ps or ∼0
3.75×10^{16}		no *o*-Ps or ∼0
5.0×10^{16}		no *o*-Ps or ∼0

The experimental errors were 0.01 ns for lifetime and 0.5% for intensity. It is clearly observed that the *o*-Ps yield exemplified by the intensity I_3 is high only for the pristine sample and the implanted samples at lower ion doses (6.25×10^{14} and 3.13×10^{15} ions/cm^2) and it suddenly decreases to 0 around 10^{16} ions/cm^2. An absence of any observable *o*-Ps yield for the implanted samples at higher ion doses (2.5×10^{16}, 3.75×10^{16}, and 5.0×10^{16} ions/cm^2) supports well the expected second process (carbonization) upon ion implantation when the ion dose is larger than 10^{16} ions/cm^2. It must be noted here that no *o*-Ps yield has been observed in carbon based materials such as, for instance, fullerene C_{60} cage[41] and carbon molecular sieve membranes.[42] The unique feature in this case is impossibility for Ps formation in the vicinity of carbon despite enough free volume space. Thus carbonization of PMMA matrix at higher ion doses leads to no positronium formation in carbonaceous phase as it is evidenced indeed from slow positron annihilation lifetime results (Table 2). These positron lifetime features at the incident positron energy of 2.15 keV correlate well with the dose dependence of *S* parameter at the same positron energy 2.15 keV and at 3.18 keV (Figure 3). As a result, all these findings obtained with slow positrons seem to account for the existence of the expected two processes, i.e., (1) *scission of polymer chains and*

dx.doi.org/10.1021/jp410763t | J. Phys. Chem. B 2014, 118, 4194−4200

appearance of free radicals preceding the aggregation of the clusters resulting in the formation of network of conjugated bonds at lower ion doses (<10^{16} ions/cm^2) and (2) *carbonization at higher ion doses (>10^{16} ions/cm^2)*.

3.2. Optical Absorption. Early UV–vis absorption spectroscopy has successfully been applied[43−46] for the characterization of structural changes of polymers after ion implantation, for example, Ag^+-implanted PMMA, ORMOCER, and epoxy resin. The authors of these publications suggested that ion irradiation creates compact carbonaceous clusters in polymers, which may also be responsible for a narrowing of optical band gap, enhanced electrical conductivity and increasing optical absorbance (see, for instance, ref 43). The increase of absorbance at lower ion doses (<10^{16} ions/cm^2) and the saturation of absorbance at higher ion doses (>10^{16} ions/cm^2) for 40 keV B:PMMA are observed in the present work, as shown in Figure 5.

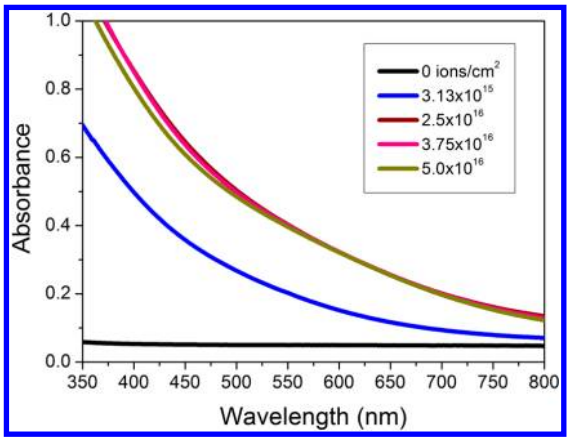

Figure 5. Optical absorption spectra of B:PMMA.

Obviously, the increasing absorbance in the course of the ion implantation in our case should be also interpreted as the signature on the formation of carbonaceous clusters. In this respect, the additional experiments with Raman and/or infrared spectroscopy to account the vibrational modes of carbonaceous clusters will be performed.

4. CONCLUSIONS

In summary, the structural defects and positronium formation in the B^+-implanted PMMA for 40 keV have been studied using SPBS, optical absorption measurements, and SRIM simulation on implanted ions and generated vacancies distribution. The obtained results of SPBS along with SRIM data are found to be clear confirmation for the concept on the occurrence of two processes upon ion implantation: scission of polymer chains and appearance of free radicals preceding the aggregation of the clusters resulting in the formation of network of conjugated bonds at lower ion doses (<10^{16} ions/cm^2) and carbonization at higher ion doses (>10^{16} ions/cm^2). The optical absorption measurements have supported these findings by slow positrons. In particular, the following main conclusions can be drawn as revealed from the present work:

(1) the results of depth distribution of implanted layer obtained by slow positrons agree with SRIM simulation;
(2) two different processes are seen on the Doppler *S* and *W* parameters as a function of positron energy in the range 0−30 keV in dependence on the ion implantation dose, namely *S*−*E* increases and *W*−*E* decreases at lower ion doses (6.25×10^{14} to 3.13×10^{15} ions/cm^2), whereas *S*−*E* decreases and *W*−*E* increases at higher ion doses (2.5×10^{16} to 5.0×10^{16} ions/cm^2);
(3) *S* parameter at incident positron energies of 2.15 and 3.18 keV decreases sharply when the ion dose exceeds 10^{16} ions/cm^2;
(4) slow positron lifetime measurements at 2.15 keV revealed that the *o*-Ps forms only for the pristine sample and the implanted samples at lower ion doses; for the implanted samples at higher ion doses there is no observable *o*-Ps yield, exemplified by the intensity I_3;
(5) optical absorption increases in the course of the ion implantation due to formation of carbonaceous phase in the B^+-irradiated PMMA.

Finally, it should be noted that the original results reported here demonstrate a high efficiency of slow positron beam spectroscopy, performed for the first time in this work for a case of ion-implanted PMMA, in combination with SRIM simulation and other experimental techniques for collecting fundamental knowledge on the ion-irradiated organic materials.

AUTHOR INFORMATION

Corresponding Author

*T. Kavetskyy: e-mail, kavetskyy@yahoo.com; phone, +38 03244 23257; fax, +38 03244 33332.

Notes

The authors declare no competing financial interest.

ACKNOWLEDGMENTS

The authors are grateful to K. Ito of AIST for enlightening suggestions. T. Kavetskyy and A. L. Stepanov acknowledge the SAIA (Slovak Academic Information Agency) for scholarships in the IPSAS within the National Scholarship Program of the Slovak Republic. O. Šauša thanks the Slovak Grant Agency VEGA for support by the grant No. 2/0099/10. S. Murata of AIST is acknowledged for the optical measurements. This work was also partly supported by the State Fund for Fundamental Researches of Ukraine (No. F52.2/003) and the Russian Foundation for Basic Research (Nos. 13-02-12012, 12-02-00528 and 12-02-97029).

REFERENCES

(1) Kavetskyy, T.; Lyadov, N.; Valeev, V.; Tsmots, V.; Petkova, T.; Boev, V.; Petkov, P.; Stepanov, A. L. *Phys. Satus Solidi C* **2012**, *9*, 2444.
(2) Wassermann, B.; Braunstein, G.; Dresselhaus, M. S.; Wenk, G. E. *Mater. Res. Soc. Symp. Proc.* **1983**, *27*, 423.
(3) Hnatowicz, V.; Kvitek, J.; Svorcik, V.; Rybka, V. *Appl. Phys. A: Mater. Sci. Process.* **1994**, *58*, 349.
(4) Guimates, R. B.; Amaral, L.; Behar, M.; Fichtner, P. F. P.; Zawislak, F. C.; Fink, D. *J. Appl. Phys.* **1988**, *63*, 2083.
(5) Fink, D.; Mueller, M.; Stettner, U.; Behar, M.; Fichner, P. F. P.; Zawislak, F. C.; Koul, S. *Nucl. Instrum. Methods B* **1988**, *32*, 150.
(6) Azarko, I. I.; Karpovich, I. A.; Kozlov, I. P.; Kozlova, E. I.; Odzhaev, V. B.; Popok, V. N.; Hnatowicz, V. *Solid State Commun.* **1995**, *95*, 49.
(7) Vacik, J.; Cervena, J.; Fink, D.; Klett, R.; Hnatowicz, V.; Popok, V.; Odzhaev, V. *Radiat. Eff. Defects Solids* **1997**, *143*, 139.
(8) Sviridov, D. V. *Russ. Chem. Rev.* **2002**, *71*, 315.
(9) Stepanov, A. L. *Tech. Phys.* **2004**, *49*, 143.
(10) Popok, V. N. *Rev. Adv. Mater. Sci.* **2012**, *30*, 1.
(11) Stepanov, A. L. In *Metal-Polymer Nanocomposites*; Nicolais, L., Carotenuto, G., Eds.; Wiley-Interscience: New York, 2005; pp 241−263.
(12) Wang, J.; Zhu, F.; Zhang, B.; Liu, H.; Jia, G.; Liu, C. *Appl. Surf. Sci.* **2012**, *261*, 653.

(13) Gupta, R.; Kumar, V.; Goyal, P. K.; Kumar, S. *Appl. Surf. Sci.* **2012**, *263*, 334.
(14) Chen, Z.; Ito, K.; Yanagishita, H.; Oshima, N.; Suzuki, R.; Kobayashi, Y. *J. Phys. Chem. C* **2011**, *115*, 18055.
(15) Liao, K.-S.; Fu, Y.-J.; Hu, C.-C.; Chen, J.-T.; Huang, Y.-H.; De Guzman, M.; Huang, S.-H.; Lee, K.-R.; Jean, Y. C.; Lai, J.-Y. *J. Phys. Chem. C* **2013**, *117*, 3556.
(16) Fujinami, M.; Suzuki, R.; Ohdaira, T.; Mikado, T. *Phys. Rev. B* **1998**, *58*, 12559.
(17) Kawasuso, A.; Arai, H.; Hirata, K.; Sekiguchi, T.; Kobayashi, Y.; Okada, S. *Radiat. Phys. Chem.* **2000**, *58*, 615.
(18) Hirata, K.; Arai, H.; Kawasuso, A.; Sekiguchi, T.; Kobayashi, Y.; Okada, S. *J. Appl. Phys.* **2001**, *90*, 237.
(19) Fujinami, M.; Miyagoe, T.; Sawada, T.; Suzuki, R.; Ohdaira, T.; Akahane, T. *Phys. Rev. B* **2003**, *68*, 165332.
(20) Chen, Z. Q.; Maekawa, M.; Yamamoto, S.; Kawasuso, A.; Yuan, X. L.; Sekiguchi, T.; Suzuki, R.; Ohdaira, T. *Phys. Rev. B* **2004**, *69*, 035210.
(21) Chen, Z. Q.; Kawasuso, A.; Xu, Y.; Naramoto, H.; Yuan, X. L.; Sekiguchi, T.; Suzuki, R.; Ohdaira, T. *Phys. Rev. B* **2005**, *71*, 115213.
(22) Brauer, G.; Anwand, W.; Skorupa, W.; Kuriplach, J.; Melikhova, O.; Moisson, C.; von Wenckstern, H.; Schmidt, H.; Lorenz, M.; Grundmann, M. *Phys. Rev. B* **2006**, *74*, 045208.
(23) Moe Børseth, T.; Tuomisto, F.; Christensen, J. S.; Monakhov, E. V.; Svensson, B. G.; Kuznetzov, A. Yu. *Phys. Rev. B* **2008**, *77*, 045204.
(24) Macchi, C.; Mariazzi, S.; Karwasz, G. P.; Brusa, R. S.; Folegati, P.; Frabboni, S.; Ottaviani, G. *Phys. Rev. B* **2006**, *74*, 174120.
(25) Moutanabbir, O.; Terreault, B.; Chicoine, M.; Schiettekatte, F.; Simpson, P. J. *Phys. Rev. B* **2007**, *75*, 075201.
(26) Slotte, J.; Rummukainen, M.; Toumisto, F.; Markevich, V. P.; Peaker, A. R.; Jeynes, C.; Gwilliam, R. M. *Phys. Rev. B* **2008**, *78*, 085202.
(27) Oliver, D. J.; Ruffel, S.; Bradby, J. E.; Williams, J. S.; Swain, M. V.; Munroe, P.; Simpson, P. J. *Phys. Rev. B* **2009**, *80*, 115210.
(28) Moutanabbir, O.; Scholz, R.; Gösele, U.; Guittoum, A.; Jungmann, M.; Butterling, M.; Krause-Rehberg, R.; Anwand, W.; Egger, W.; Sperr, P. *Phys. Rev. B* **2010**, *81*, 115205.
(29) Anto, C. V.; Abhaya, S.; Magudapathy, P.; Amarendra, G.; Nair, K. G. M. *J. Phys. D: Appl. Plys.* **2010**, *43*, 325401.
(30) Dong, Y.; Toumisto, F.; Svensson, B. G.; Kuznetzov, A.Yu.; Brillson, L. J. *Phys. Rev. B* **2010**, *81*, 081201(R).
(31) Neuvonen, P. T.; Vines, L.; Venkatachalapathy, V.; Zubiaga, A.; Tuomisto, F.; Hallén, A.; Svensson, B. G.; Kuznetsov, A.Yu. *Phys. Rev. B* **2011**, *84*, 205202.
(32) *Positron Spectroscopy of Solids*; Dupasquier, A., Mills, A.P., Jr., Eds.; Proceedings of the International School of Physics "Enrico Fermi", Course CXXV; IOS Press: Amsterdam, 1995.
(33) He, C.; Wang, S.; Kobayashi, Y.; Ohdaira, T.; Suzuki, R. *Phys. Rev. B* **2012**, *86*, 075415.
(34) Kobayashi, Y.; Kojima, I.; Hishita, S.; Suzuki, T.; Asari, E.; Kitajima, M. *Phys. Rev. B* **1995**, *52*, 823.
(35) Suzuki, R.; Ohdaira, T.; Mikado, T.; Ohgaki, H.; Yamasaki, T.; Chiwaki, M. *Appl. Surf. Sci.* **1997**, *116*, 187.
(36) Ziegler, J. F.; Biersak, J. P.; Littmark, U. *The Stopping and Range of Ions in Solids*; Pergamon: New York, 1996; http://www.srim.org.
(37) Hirata, K.; Kobayashi, Y.; Hishita, S.; Ujihira, Y. *Appl. Phys. A: Mater. Sci. Process.* **1997**, *64*, 491.
(38) Kobayashi, Y.; Ito, K.; Oka, T.; He, C.; Mohamed, H. F. M.; Suzuki, R.; Ohdaira, T. *Appl. Surf. Sci.* **2008**, *255*, 174.
(39) Zhang, L.; Townsend, P. D.; Chandler, P. J.; Kulish, J. R. *J. Appl. Phys.* **1989**, *66*, 4547.
(40) Sato, K.; Ito, K.; Hirata, K.; Yu, R. S.; Kobayashi, Y. *Phys. Rev. B* **2005**, *71*, 012201.
(41) Krištiak, J.; Krištiakova, K.; Šauša, O. *Phys. Rev. B* **1994**, *50*, 2792.
(42) Liao, K.-S.; Fu, Y.-J.; Hu, C.-C.; Chen, J.-T.; Lin, D.-W.; Lee, K.-R.; Tung, K.-L.; Jean, Y. C.; Lai, J.-Y. *Carbon* **2012**, *50*, 4220.
(43) Stepanov, A. L.; Abdullin, S. N.; Petukhiv, V. Y.; Osin, Y. N.; Khaibullin, R. I.; Khaibullin, I. B. *Philos. Mag. B* **2000**, *80*, 23.
(44) Stepanov, A. L.; Kiyan, R.; Ovsianikov, A.; Nuzhdin, V. I.; Valeev, V. F.; Osin, Y. N.; Chichkov, B. N. *Appl. Phys. A: Mater. Sci. Process.* **2012**, *108*, 375.
(45) Stepanov, A. L. In *Wiley Encyclopedia of Composites*; Nicolais, L., Borzacchiello, A., Eds.; Wiley-Interscience: New York, 2012; pp 1045–1058.
(46) Takele, H.; Greve, H.; Pochstein, C.; Zaporojtchenko, V.; Faupel, F. *Nanotechnology* **2006**, *17*, 3499.